RSC Advances

This article can be cited before page numbers have been issued, to do this please use: W. Wang, C. Lai, Y. Lin, T. Yu, Z. Chen, W. Wu and P. Yeh, *RSC Adv.*, 2016, DOI: 10.1039/C6RA09033H.

Surface Defects Engineering: Gigantic Enhancement in the Optical and Gas Detection Ability of Metal Oxide Sensor

Wen-Chieh Wang[a†], Chun-Yen Lai[b†], Yu-Ting Lin[a], Tzu-Hsuan Yua[a], Zong-Yi Chen[a], Wen-Wei Wu[b] and Ping-Hung Yeh[*a]

[a] Department of Physics, Tamkang University, Tamsui, New Taipei City, 25137, Taiwan

View Article Online
DOI: 10.1039/C6RA09033H

[b] Department of Materials Science and Engineering, National Chiao Tung University, No. 1001, University Road, East District, Hsinchu City 30010, Taiwan

[†]First two authors contribute to this work equally.

[*] Prof. Ping-Hung Yeh Corresponding-Author,

E-mail: ((phyeh331@mail.tku.edu.tw))

ABSTRACT

In this work, the detection ability of nanosensors can be improved extraordinary by surface defects engineering. The kinked SnO_{2-X} /SnO_2 nanostructure was fabricated by tuning the oxygen flow and used this kinked SnO_{2-X} /SnO_2 nanostructure to study the mechanism of surface defect (oxygen vacancy, V_O) affection through the electric measurement. For UV light sensing, the response of SnO_{2-X} NW device is always better than SnO_2 NW device, two orders higher under pure O_2 surrounding condition. The detection mechanism can be clarified by changing the detection environment (oxygen concentration) and the UV light detection sensitivity can be improved by increasing the surface V_O density. Furthermore, the SnO_{2-X} NW device is very sensitive to its surrounding environment due to the high surface V_O density. Hence, the CO/O$_2$ alternate-detection was used to verify our hypothesis; the results show that the SnO_{2-X} NW device presents great detection ability, compared with SnO_2 NW device. The sensitivity of SnO_{2-X} NW device is two orders enhancements and the reset/response time is faster, compared with SnO_2 NW device. To verify this

hypothesis, the polycrystalline structure was fabricated to prove that the detection ability of metal-oxide nanosensors can be improved gigantically by increasing surface defect amount.

Keywords: surface defect, low temperature gas detection, metal-oxide

Introduction

Recently, nanomaterials, such as nanowire[1-4], nanobelt[5-7] and nanotube[8-10], polymer material[11], have been extensively studied and utilized to form nano-devices for different application[12-18]. For metal-oxide nanomaterials, because the high surface-to-volume ratio and surface defect of nanostructures, which made the metal-oxide nanomaterials are quite sensitive for the environment variation[19-26]. Many articles reported that Schottky contact mechanism can enhance the performance of metal-oxide nanomaterials, such as piezotronic devices[27, 28], nanogenerators[29-32] and nanosensors[20, 33-39].

View Article Online
DOI: 10.1039/C6RA09033H

For sensor application, using Schottky contact as a control gate can improve the sensitivity, response and reset time[39-42]. Besides, the defect amount of metal-oxide nanomaterials is main parameter for sensor application[43-49]. The surface defect[50] and the oxygen vacancy[51] of meta-oxide nanomaterials have been reported and discussed widely. Many research works tried to control the defect amount and level of metal-oxide in chemical or physical way to create other possibility or application[52-60]. Besides, the signal output of Schottky contact device is strong relative to the surface defect.

Tin dioxide, SnO_2, which has potential for ultraviolet (UV) light detection application, due to its large band gap[61]. Otherwise, SnO_2 is also a candidate for gas detection because the oxygen vacancy[18, 39, 48, 57, 58]. Besides, SnO_2 also can be used as photo-catalyst and solar-cell applications[55, 62-64]. In this research work, the Tin oxide nanomaterials were fabricated with different amounts of defect; and the devices were formed as a Schottky gate device for the mechanism investigation. The relativity of the detection ability and defect amount of Tin oxide nanosensor can be figure out by using the Schottky contact devices made with this kinked structure.

Results and discussion

The detail analyses of Tin oxide nanostructure (NS) can be obtained from the TEM images, as shown in

Figure 1. The growth direction of Tin oxide NS can be identified from the diffraction pattern and high resolution TEM images, as shown in Figure 1a~c. Due to our synthesis controlling, the oxygen composition of both side would be different; the lower oxygen composition was detected for the NS growth without oxygen flow, as shown in (d)~(f). The schematic and SEM images of nanodevice can be seen in Figure 1 (g). The Pt was deposited by focus ion beam (FIB) to form Ohmic contact; the free contacts of both sides can be formed to be Schottky contacts as detection units[65]. Each side composition of nanodevice can be identified by EDS of SEM system, as illustrated in Figure 1 (h).

View Article Online
DOI: 10.1039/C6RA09033H

For photodetection, the sensitivity of SnO_{2-X} NW device for UV (254nm) light detection is higher than SnO_2 NW device; because the dark current (I_D) of SnO_{2-X} NW device is smaller than the I_D of SnO_2 NW device and the photo current (I_P) of SnO_{2-X} NW device is larger than the I_P of SnO_2 NW device, respectively, as shown in Figure 2 (a). The temperature of measurement is in room temperature, 25℃. The UV detection ability of both devices is related to the oxygen concentration of sensing environment, as illustrated in Figure 2 (b). The sensitivity of SnO_{2-X} NW device is always higher than SnO_2 NW device, no matter what oxygen concentration percentage is. The UV detection sensitivity of both NW devices will be increased when the oxygen concentration increasing. The sensing mechanism can be illustrated as Figure 2 (c) and (d) for each device.

The SnO_{2-X} NW device has impressive improvement of sensitivity is because that the density of surface oxygen vacancy (V_O) is higher. When the UV light off, the SnO_{2-X} NW device would trap more oxygen molecules at Schottky contact interface to form O_2^- and raise the Schottky barrier height (SBH) to reduce the current, so the I_D of SnO_{2-X} NW device would be lower than SnO_2 NW device. But when the UV light on, the electron-hole pair would be generated and O_2^- would be desorbed by the hole. Because the hole would combine with the O_2^- to form $O_{2(g)}$ and desorb, that would reduce the SBH to increase the I_P. Besides, the lone pair electrons will increase the I_P of SnO_{2-X} NW device, compare with SnO_2 NW device, the lone pair electrons amount of SnO_{2-X} NW device is larger, as shown in Figure 2 (c) and (d). Due to above-mentioned

results, the response can be improved no matter what oxygen concentration by using the SnO_{2-X} NW device, compare with SnO_2 NW device. The SBH variation also can be analyzed from the electrical measurement, the $\Delta\Phi$ (SBH variation) would be stabled for SnO_2 NW device after 40 % oxygen concentration. But for SnO_{2-X} NW device, the $\Delta\Phi$ would be raised with the concentration of oxygen increasing, as shown in Figure 2 (e). The SBH can be approximately presented by the following equation[66]:

$$I_r = AA^{**2} exp[-q\Phi_{eff}/kT]$$

View Article Online DOI: 10.1039/C6RA08833H

Here, I_r is the reverse bias we set, A is the contact area between SnO_2 NW and Pt electrode, A^{**} is the effective Richardson Constant, q is electric charge, Φ_{eff} is the SBH, k and T is the Boltzmann Constant and system temperature, respectively.

The $\Delta\Phi$ of both devices are almost the same for the oxygen concentration around 20%; but when the oxygen concentration above 40%, the $\Delta\Phi$ would be different. This result symbolizes the surface V_O density of SnO_{2-X} NW device is higher than the SnO_2 NW device based on the mechanism illustrated in Figure 2 (c) and (d), which also consists with the TEM and SEM analyses. The SBH differences can be measured and analyzed between SnO_{2-X} and SnO_2 NW devices by oxygen concentration variation, and the difference will be enlarged when the oxygen concentration increasing as shown in Table 1 (Detail measurement can be seen in Figure S1). Above result shows that the Tin oxide based NW device would be very sensitive to its surrounding environment, especially for oxygen concentration. So we can presume that Tin oxide based NW device will have great detection ability for gas, especially for SnO_{2-X} NW device.

From our data, the gas detection ability of SnO_{2-X} NW device is better than the SnO_2 NW device, as shown in Figure 3. For gas detection, the O_2-detection current density (J) was used for base current ($J_0=J_{O_2}$) and the CO-detection current density (J_{CO}) was used for reaction current ($J=J_{CO}$). The sensitivity (S) can be defined as $S=\Delta J/J_0$, $\Delta J=J_{CO}- J_{O_2}$. For sensing, the CO detection signal output of SnO_{2-X} NW device is larger than SnO_2 NW device, and the J_0 of SnO_{2-X} NW device is smaller than SnO_2 NW device, can be seen in Figure 3 (a). So that the sensitivity of SnO_{2-X} NW device is higher than SnO_2 NW device for each individual

CO concentration detection, as shown in Figure 3 (b). The repetition of both devices can be seen for 2 ppm CO detection can be seen in Figure S3. The detection mechanism can be described in Figure 3 (c). Because the high surface V_O density of SnO_{2-X} NW device, the J_{O_2} can be reduced due to SBH raising since oxygen adsorption. Considering CO/O_2 alternate-detection, the SBH variation of SnO_{2-X} NW device is larger than SnO_2 NW device. Based on this surface V_O density difference, the improvement of the gas detection abilities (the sensitivity, response and reset time) of SnO_{2-X} NW device are gigantic, compared with SnO_2 NW device. From Table 2, we can see higher sensitivity and faster reset time since increasing the CO concentration by using SnO_{2-X} NW device (Detail data can be seen in Figure S2). That is because larger CO concentration can reduce more SBH to have higher current (J_{CO}); so when the O_2 flow in to raise the SBH, the current (J_{O_2}) will be decreased immediately. But the response time is related to the influence of gas-surface interaction, the interaction most depend on the temperature effect. So the response time will be no related with different CO concentration. This results can support our hypothesis, which increasing surface defects can improve the response. So we synthesized another polycrystalline nanostructure to reconfirm our hypothesis. The polycrystalline structure we use is SnO_2 (p-SnO_2) and ZnO (p-ZnO) nanowire to compare with single-crystalline SnO_2 (s- SnO_2). The sensitivity enhancements of p-SnO_2 and p-ZnO are two order larger than s-SnO_2 by the UV light detection; The sensitivities of s-SnO_2, p-SnO_2 and p-ZnO are 9.4 %, 132.3 % and 130.7 %, as seen in Figure S4.

View Article Online
DOI: 10.1039/C6RA09033H

Experiment

Asymmetric kinked SnO_2 /SnO_{2-X} nanowires

The kinked SnO_{2-X}/SnO_2 NWs were synthesized on silicon substrates at 850 ^oC via the general catalyst free thermal evaporation method using SnO_2 and carbon powders as sources in a horizontal quartz tube connected to vacuum pump and a programmable mass flow controller (MFC). The source was placed in an alumina boated located at the high temperature zone 1000 ^oC. The substrates then positioned in the source downstream. After the tube had been sealed and evacuated to the base pressure, a carrier gas, Ar/O_2, was kept flowing through the tube to direct the deposition process. Initially, SnO_2 NWs were grown in 10

standard cubic cemtimeters per minute (s.c.c.m.) Ar/O_2 mixture gas with the volume ratio of 5:1 for 15 min to create the stoichiometric SnO_2 segment, as shown in Figure S5. After reaction, the oxygen input was turned off, and the background pressure was kept at 4 torr to create the SnO_{2-X} segment. The growth plane of the kinked NW shifts from (200) to (002) owing to the external pressure perturbation.

Conclusions

In this research work, we have demonstrated that the kinked SnO_{2-X}/SnO_2 nanostructure can be forme

View Article Online
DOI: 10.1039/C6RA09033H

by controlling the oxygen flow; used this kinked SnO_{2-X}/SnO_2 nanostructure to form Schottky contact devices and to study the affection of the surface V_O density through the optical and gas condition electric measurement. For UV light detection, the gigantic enhancement in sensitivity of SnO_{2-X} NW device is because the V_O can generate more electron-hole pairs to improve the photo response. We also studied the mechanism by controlling the detection environment (oxygen concentration) and we figured out that the $\Delta\Phi$ is related with oxygen concentration. Based on this result, we found that the SnO_{2-X} NW device is quite sensitive to its surrounding environment. So we used the CO/O_2 alternate-detection to verify our hypothesis and the results show that the SnO_{2-X} NW device presents great detection ability, compared with SnO_2 NW device. The sensitivities of the SnO_{2-X} NW device are two order larger than the SnO_2 NW device when CO concentration over 50 ppm. The response and reset time all improved by using the SnO_{2-X} NW device. We proved that increasing the surface defects and using Schottky contact can improve the detection ability of metal-oxide nanosensors extraordinary. Based on above idea, we also designed another nanostructure, polycrystalline nanostructure, to reconfirm the hypothesis. The sensitivities of p-SnO_2.and p-ZnO devices are 132.3 % and 130.7 %, all perform better than s-SnO_2, 9.4 %. We can use the technology of material science engineering and physics to design high-resolution and fast monitor speed nanosensor.

Acknowledgements

This research was supported by the Ministry of Science and Technology, Taiwan, under grants NSC-101-2112-M-032-004-MY3 and MOST-104-2112-M-032-003-006

Figure captions

Figure 1. (a) Low magnification TEM image of a kinked SnO_{2-X}/SnO_2 nanostructure with the growth orientation changed from (200) to (002), the growth orientation can be indicated by the selected area electron diffraction (SAED) pattern in the inset. (b) and (c) show the high resolution images and lattice constant of SnO_2 and SnO_{2-X}, respectively. (d) The Sn and O concentrations of a kinked SnO_{2-X}/SnO_2 nanowire can be analyzed by EDS element line scan. (e) and (f) show the elemental mapping of Sn and O, respectively. (g) Schematic diagram and SEM image of SnO_{2-X}/SnO_2 nanowire Schottky contacted device. (h) EDS analysis and the atomic percent data of SnO_{2-X}/SnO_2 NWs.

Figure.2 (a) 254nm UV detection performance in 40% oxygen gas environment (with 40% oxygen and 60% nitrogen). (b) The sensitivities in different oxygen concentration of SnO_{2-X} and SnO_2 NW devices. (c) and (d) show the mechanism diagrams of SnO_{2-X} and SnO_2 NW devices of oxygen molecules interaction at the interface. Step (i) and (ii) represent the adsorption of oxygen molecules. (iii) shows the desorption of oxygen molecules by UV illumined. The SnO_{2-X} NW device has higher sensitivity is because that the V_O is higher. When the UV light off, more oxygen molecules were trapped at Schottky contact interface to form O_2^- and raise the Schottky batrrier height (SBH) to reduce the current, so the I_d of SnO_{2-X} NW device was lower. But turn on the UV light, the electron-hole pairs would be generated and O_2^- would be desorbed by the hole. Because the hole would combine with the O_2^- to form $O_{2(g)}$ and desorb, that would reduce the SBH to increase the I_P. (e) The variation of SBH from vacuum environment to pure oxygen environment (with 100% oxygen) of SnO_{2-X} and SnO_2 NW devices.

Figure.3 (a) represents detection performance of O_2 with different CO concentration sensing at 200 °C operation temperature. (b) The sensitivities of SnO_{2-X} NW device are higher than SnO_2 NW device for different CO concentrations detection. (c) shows the detection mechanism of SnO_{2-X} and SnO_2 NW devices. Considering CO/O_2 alternate-detection, the SBH variation of SnO_{2-X} NW device is larger than SnO_2 NW device ($\Delta\Phi_{SnO_{2-X}} > \Delta\Phi_{SnO_2}$), that is due to the high surface V_O density of SnO_{2-X} NW device.

Table 1. The variation and difference of two schottky barrier height in different O_2 concentration environment.

Oxygen concentration (y%)	$\Delta\Phi_{y\%-y\text{-}20\%}$		$\Phi_{SnO_{2-x}} - \Phi_{SnO_2}$
	SnO_{2-X}	SnO_2	
0%	-	-	-
20%	85 meV	83 meV	2 meV
40%	27 meV	21 meV	8 meV
60%	6 meV	3 meV	11 meV
80%	18 meV	5 meV	25 meV
100%	26 meV	4 meV	47 meV

View Article Online
DOI: 10.1039/C6RA09033H

Table 2. The sensitivity, response time and reset time of different CO concentration gas sensing.

CO concentration		Sensitivity	$\tau_{response}$	τ_{reset}
2 ppm	SnO_{2-X}	490 % ± 43 %	169 s	221 s
	SnO_2	75 % ± 7 %	180 s	238 s
50 ppm	SnO_{2-X}	27549 % ± 1521 %	234 s	7 s
	SnO_2	254 % ± 53 %	451 s	9 s
100 ppm	SnO_{2-X}	43657 % ± 2232 %	420 s	2 s
	SnO_2	541 % ± 124 %	630 s	3 s
200 ppm	SnO_{2-X}	46726 % ± 780 %	225 s	<1 s
	SnO_2	551 % ± 76 %	341 s	2 s

References

1. S. Xu and Z. Wang, *Nano Res.*, 2011, **4**, 1013-1098.
2. P. Gao and Z. Wang, in *Scanning Microscopy for Nanotechnology*, Springer New York, 2007, ch. 13, pp. 384-426.
3. Ü. Özgür, Y. I. Alivov, C. Liu, A. Teke, M. A. Reshchikov, S. Doğan, V. Avrutin, S. J. Cho and H. Morkoç, *J. Appl. Phys.*, 2005, **98**, 041301.
4. Z. Wang, *Chinese Sci. Bull.*, 2009, **54**, 4021-4034.
5. J. Wang, D. N. Tafen, J. P. Lewis, Z. Hong, A. Manivannan, M. Zhi, M. Li and N. Wu, *J. Am. Chem. Soc.*, 2009, **131**, 12290-12297.
6. K. Shankar, J. I. Basham, N. K. Allam, O. K. Varghese, G. K. Mor, X. Feng, M. Paulose, J. A. Seabold, K.-S. Choi and C. A. Grimes, *J. Phys. Chem. C*, 2009, **113**, 6327-6359.
7. O. Lupan, T. Braniste, M. Deng, L. Ghimpu, I. Paulowicz, Y. K. Mishra, L. Kienle, R. Adelung and I. Tiginyanu, *Sensor. Actuat. B-Chem.*, 2015, **221**, 544-555.
8. G. She, X. Huang, L. Jin, X. Qi, L. Mu and W. Shi, *Small*, 2014, **10**, 4685-4692.
9. S. Y. Yang, W. Choi and H. Park, *ACS Appl. Mater. Interfaces*, 2015, **7**, 1907-1914.
10. D. H. Kim, Y.-S. Shim, J.-M. Jeon, H. Y. Jeong, S. S. Park, Y.-W. Kim, J.-S. Kim, J.-H. Lee and H. W. Jang, *ACS Appl. Mater. Interfaces*, 2014, **6**, 14779-14784.
11. Y. Gao, Y. Zhao, L. Qiu, Z. Guo, D. O'Hare and Q. Wang, *Polymer Composites*, 2015, DOI: 10.1002/pc.23764.
12. X. Wang, N. Aroonyadet, Y. Zhang, M. Mecklenburg, X. Fang, H. Chen, E. Goo and C. Zhou, *Nano Lett.*, 2014, **14**, 3014-3022.
13. L. Peng, L. Hu and X. Fang, *Adv. Funct. Mater.*, 2014, **24**, 2591-2610.
14. S. Jeong, M. Choe, J.-W. Kang, M. W. Kim, W. G. Jung, Y.-C. Leem, J. Chun, B.-J. Kim and S.-J. Park, *ACS Appl. Mater. Interfaces*, 2014, **6**, 6170-6176.
15. A. Pescaglini, A. Martín, D. Cammi, G. Juska, C. Ronning, E. Pelucchi and D. Iacopino, *Nano Lett.*, 2014, **14**, 6202-6209.
16. X. Yang, R. Liu, C. Du, P. Dai, Z. Zheng and D. Wang, *ACS Appl. Mater. Interfaces*, 2014, **6**, 12005-12011.
17. N. A. Kyeremateng, *ChemElectroChem*, 2014, **1**, 1442-1466.
18. M. Law, H. Kind, B. Messer, F. Kim and P. Yang, *Angewandte Chemie*, 2002, **114**, 2511-2514.
19. G. F. Fine, L. M. Cavanagh, A. Afonja and R. Binions, *Sensors*, 2010, **10**.
20. Z. Yang, X. Dou, S. Zhang, L. Guo, B. Zu, Z. Wu and H. Zeng, *Adv. Funct. Mater.*, 2015, **25**, 4039-4048.
21. H. S. Woo, C. H. Kwak, J. H. Chung and J. H. Lee, *ACS Appl. Mater. Interfaces*, 2014, **6**, 22553-22560.
22. S. W. Choi, A. Katoch, G. J. Sun, J. H. Kim, S. H. Kim and S. S. Kim, *ACS Appl. Mater. Interfaces*, 2014, **6**, 8281-8287.
23. A. Katoch, J. H. Kim and S. S. Kim, *ACS Appl. Mater. Interfaces*, 2014, **6**, 21494-21499.
24. H. Zhou, R. Deng, Y.-F. Li, B. Yao, Z.-H. Ding, Q.-X. Wang, Y. Han, T. Wu and L. Liu, *J. Phys. Chem. C*, 2014, **118**, 6365-6371.
25. F. Hernández-Ramírez, J. Rodríguez, O. Casals, E. Russinyol, A. Vilà, A. Romano-Rodríguez, J. R. Morante and M. Abid, *Sensor. Actuat. B-Chem.*, 2006, **118**, 198-203.
26. F. Hernández-Ramírez, A. Tarancón, O. Casals, J. Arbiol, A. Romano-Rodríguez and J. R. Morante, *Sensor. Actuat. B-Chem.*, 2007, **121**, 3-17.
27. Z. L. Wang, in *Piezotronics and Piezo-Phototronics*, Springer Berlin Heidelberg, 2012, ch. 1, pp. 1-17.
28. R. Yu, C. Pan, J. Chen, G. Zhu and Z. L. Wang, *Adv. Funct. Mater.*, 2013, **23**, 5868-5874.
29. W. Seung, M. K. Gupta, K. Y. Lee, K.-S. Shin, J.-H. Lee, T. Y. Kim, S. Kim, J. Lin, J. H. Kim and S.-W. Kim,

ACS Nano, 2015, **9**, 3501-3509.
30. L. W. Yamin, in *Piezoelectric ZnO Nanostructure for Energy Harvesting*, John Wiley & Sons, Inc., 2015, ch. 4, pp. 65-103.
31. S. Garain, T. K. Sinha, P. Adhikary, K. Henkel, S. Sen, S. Ram, C. Sinha, D. Schmeißer and D. Mandal, *ACS Appl. Mater. Interfaces*, 2015, **7**, 1298-1307.
32. Y. Wu, Q. Jing, J. Chen, P. Bai, J. Bai, G. Zhu, Y. Su and Z. L. Wang, *Adv. Funct. Mater.*, 2015, **25**, 2166-2174.
33. T.-Y. Wei, P.-H. Yeh, S.-Y. Lu and Z. L. Wang, *J. Am. Chem. Soc.*, 2009, **131**, 17690-17695.
34. C. Pan, R. Yu, S. Niu, G. Zhu and Z. L. Wang, *ACS Nano*, 2013, **7**, 1803-1810.
35. Y. Hu, J. Zhou, P. H. Yeh, Z. Li, T. Y. Wei and Z. L. Wang, *Adv. Mater*, 2010, **22**, 3327-3332.
36. P. Chinnamuthu, J. C. Dhar, A. Mondal, A. Bhattacharyya and N. K. Singh, *J. Phys. D: Appl. Phys.*, 2012, **45**, 135102.
37. S. Lenaerts, J. Roggen and G. Maes, *Spectrochimica Acta Part A: Molecular and Biomolecular Spectroscopy*, 1995, **51**, 883-894.
38. E. R. Viana, J. C. González, G. M. Ribeiro and A. G. de Oliveira, *J. Phys. Chem. C*, 2013, **117**, 7844-7849.
39. C.-M. Chang, C.-H. Hsu, Y.-W. Liu, T.-C. Chien, C.-H. Sung and P.-H. Yeh, *Nanoscale*, 2015, **7**, 20126-20131.
40. Y.-H. Zhang, L.-F. Han, Y.-H. Xiao, D.-Z. Jia, Z.-H. Guo and F. Li, *Computational Materials Science*, 2013, **69**, 222-228.
41. C.-H. Sung, T.-C. Chien, C.-M. Chang, C.-M. Chang and P.-H. Yeh, *RSC Adv.*, 2015, **5**, 16769-16773.
42. J. K. Hsu, T. Y. Lin, C. Y. Lai, T. C. Chien, J. H. Song and P. H. Yeh, *Appl. Phys. Lett.*, 2013, **103**, 123507.
43. N. O. Savage, S. A. Akbar and P. K. Dutta, *Sensor. Actuat. B-Chem.*, 2001, **72**, 239-248.
44. C. S. Moon, H.-R. Kim, G. Auchterlonie, J. Drennan and J.-H. Lee, *Sensor. Actuat. B-Chem.*, 2008, **131**, 556-564.
45. Q. H. Li, T. Gao, Y. G. Wang and T. H. Wang, *Appl. Phys. Lett.*, 2005, **86**, 123117.
46. S. Mathur, S. Barth, H. Shen, J.-C. Pyun and U. Werner, *Small*, 2005, **1**, 713-717.
47. M. K. Nowotny, L. R. Sheppard, T. Bak and J. Nowotny, *J. Phys. Chem. C*, 2008, **112**, 5275-5300.
48. S. Das and V. Jayaraman, *Progress in Materials Science*, 2014, **66**, 112-255.
49. J. Nisar, Z. Topalian, A. De Sarkar, L. Österlund and R. Ahuja, *ACS Appl. Mater. Interfaces*, 2013, **5**, 8516-8522.
50. G. Pacchioni, *Physical Chemistry Chemical Physics*, 2013, **15**, 1737-1757.
51. X. Pan, M.-Q. Yang, X. Fu, N. Zhang and Y.-J. Xu, *Nanoscale*, 2013, **5**, 3601-3614.
52. C. Shoou-Jinn, H. Ting-Jen, I. C. Chen and H. Bohr-Ran, *Nanotechnology*, 2008, **19**, 175502.
53. J. M. Wu, Y.-R. Chen and W. T. Kao, *ACS Appl. Mater. Interfaces*, 2014, **6**, 487-494.
54. A. Kar, S. Kundu and A. Patra, *J. Phys. Chem. C*, 2010, **115**, 118-124.
55. Y. Zhang, A. Kolmakov, S. Chretien, H. Metiu and M. Moskovits, *Nano Lett.*, 2004, **4**, 403-407.
56. S. Bhaumik, A. K. Sinha, S. K. Ray and A. K. Das, *IEEE Trans. Magn.*, 2014, **50**, 1-6.
57. J. Pan, R. Ganesan, H. Shen and S. Mathur, *J. Phys. Chem. C*, 2010, **114**, 8245-8250.
58. F. Hernandez-Ramirez, J. D. Prades, A. Tarancon, S. Barth, O. Casals, R. Jimenez-Diaz, E. Pellicer, J. Rodriguez, J. R. Morante, M. A. Juli, S. Mathur and A. Romano-Rodriguez, *Adv. Funct. Mater.*, 2008, **18**, 2990-2994.
59. M. Epifani, J. D. Prades, E. Comini, E. Pellicer, M. Avella, P. Siciliano, G. Faglia, A. Cirera, R. Scotti, F. Morazzoni and J. R. Morante, *J. Phys. Chem. C*, 2008, **112**, 19540-19546.
60. H. Zeng, G. Duan, Y. Li, S. Yang, X. Xu and W. Cai, *Adv. Funct. Mater.*, 2010, **20**, 561-572.
61. W. Zhou, Y. Liu, Y. Yang and P. Wu, *J. Phys. Chem. C*, 2014, **118**, 6448-6453.

62. Y. Li, J. Zhu, Y. Huang, F. Liu, M. Lv, S. Chen, L. Hu, J. Tang, J. Yao and S. Dai, *RSC Adv.*, 2015, **5**, 28424-28429.
63. X. Li, Q. Yu, C. Yu, Y. Huang, R. Li, J. Wang, F. Guo, Y. Zhang, S. Gao and L. Zhao, *Journal of Materials Chemistry A*, 2015, **3**, 8076-8082.
64. J. Song, E. Zheng, J. Bian, X.-F. Wang, W. Tian, Y. Sanehira and T. Miyasaka, *Journal of Materials Chemistry A*, 2015, **3**, 10837-10844.
65. P. H. Yeh, Z. Li and Z. L. Wang, *Adv. Mater*, 2009, **21**, 4975-4978.
66. S. M. Sze, *Physics of Semiconductor Devices*, 1981.

View Article Online
DOI: 10.1039/C6RA09033H

Title: Surface Defects Engineering: Gigantic Enhancement in the Optical and Gas Detection Ability of Metal Oxide Sensor

ToC figure: By using the surface defect engineering, the UV and gas detection abilities can be improved.

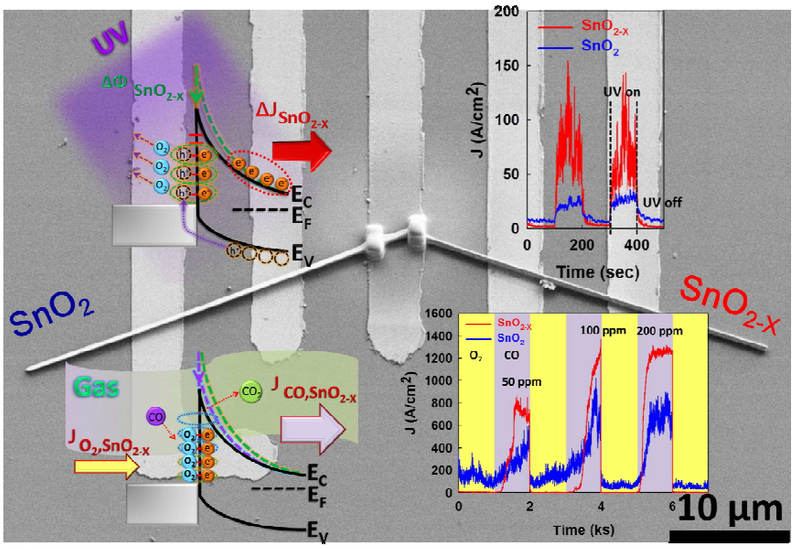

View Article Online
DOI: 10.1039/C6RA09033H

View Article Online
DOI: 10.1039/C6RA09033H

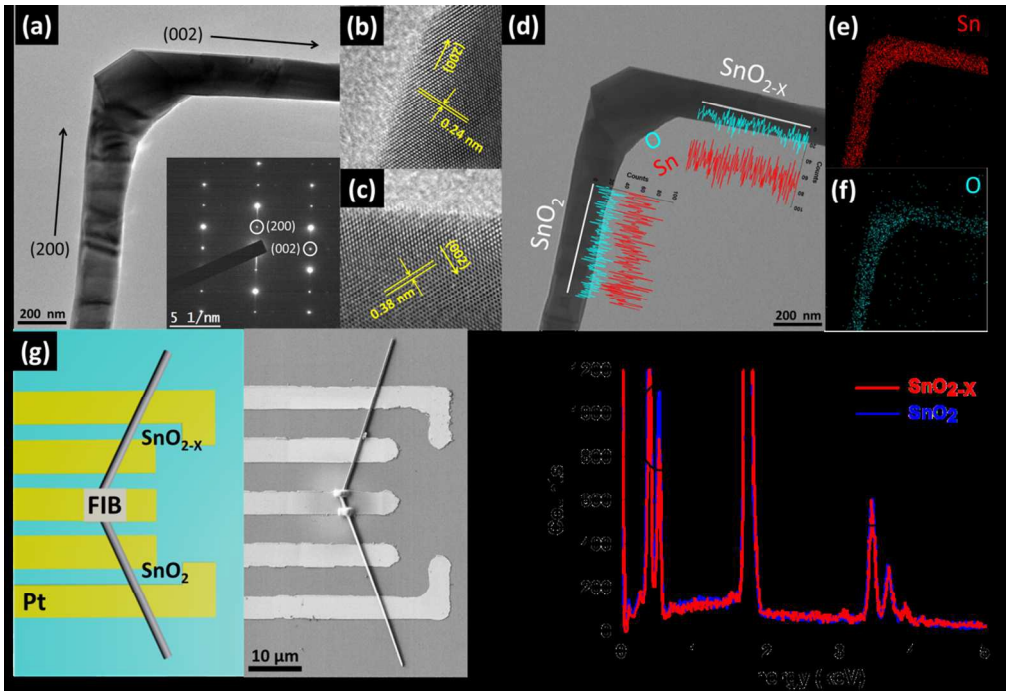

Figure 1. (a) Low magnification TEM image of a kinked SnO2-X/SnO2 nanostructure with the growth orientation changed from (200) to (002), the growth orientation can be indicated by the selected area electron diffraction (SAED) pattern in the inset. (b) and (c) show the high resolution images and lattice constant of SnO2 and SnO2-X, respectively. (d) The Sn and O concentrations of a kinked SnO2-X/SnO2 nanowire can be analyzed by EDS element line scan. (e) and (f) show the elemental mapping of Sn and O, respectively. (g) Schematic diagram and SEM image of SnO2-X/SnO2 nanowire Schottky contacted device. (h) EDS analysis and the atomic percent data of SnO2-X/SnO2 NWs.
149x102mm (220 x 220 DPI)

View Article Online
DOI: 10.1039/C6RA09033H

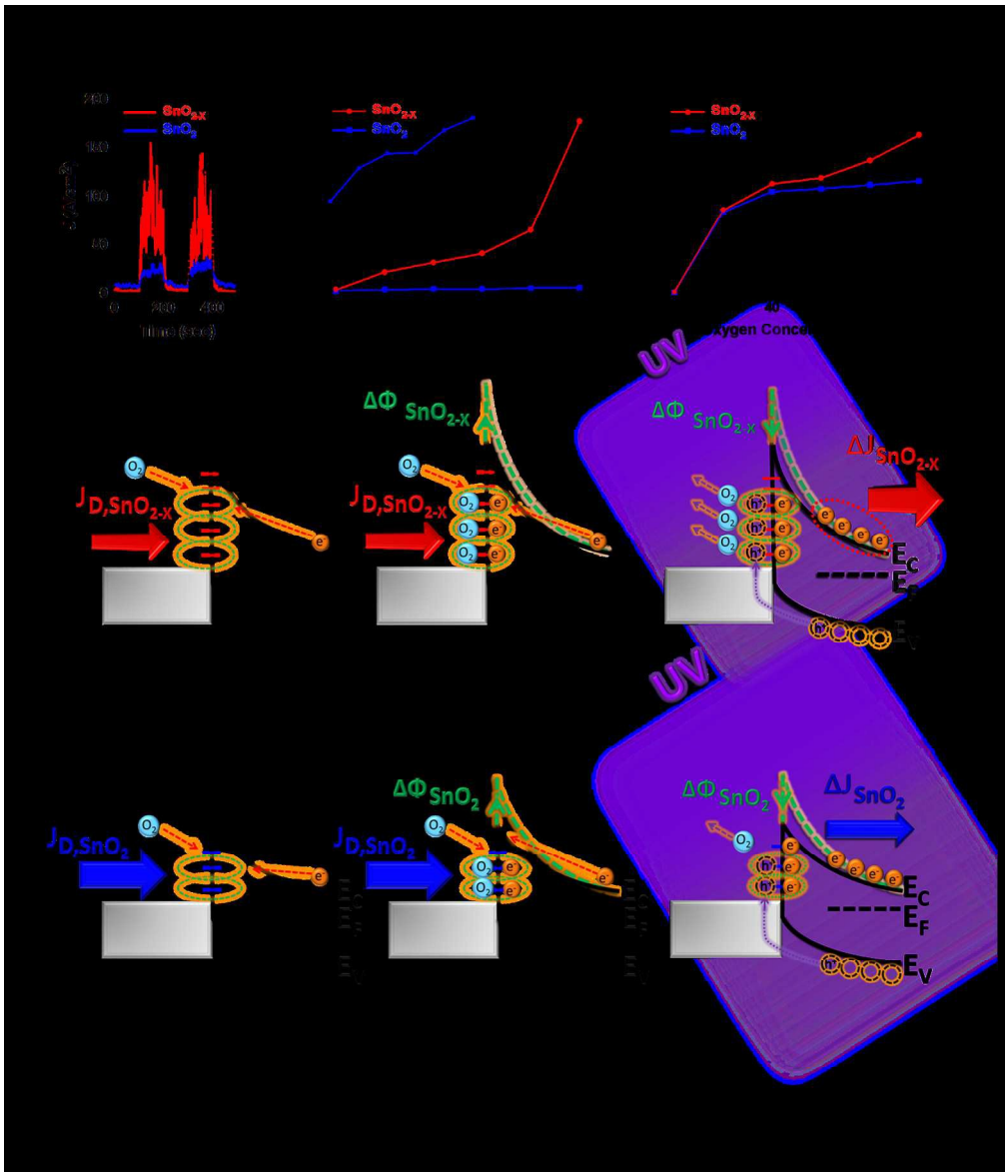

Figure.2 (a) 254nm UV detection performance in 40% oxygen gas environment (with 40% oxygen and 60% nitrogen). (b) The sensitivities in different oxygen concentration of SnO2-X and SnO2 NW devices. (c) and (d) show the mechanism diagrams of SnO2-X and SnO2 NW devices of oxygen molecules interaction at the interface. Step (i) and (ii) represent the adsorption of oxygen molecules. (iii) shows the desorption of oxygen molecules by UV illumined. The SnO2-X NW device has higher sensitivity is because that the VO is higher. When the UV light off, more oxygen molecules were trapped at Schottky contact interface to form O2- and raise the Schottky batrrier height (SBH) to reduce the current, so the Id of SnO2-X NW device was lower. But turn on the UV light, the electron-hole pairs would be generated and O2- would be desorbed by the hole. Because the hole would combine with the O2- to form O2(g) and desorb, that would reduce the SBH to increase the IP. (e) The variation of SBH from vacuum environment to pure oxygen environment (with 100% oxygen) of SnO2-X and SnO2 NW devices.
350x408mm (150 x 150 DPI)

View Article Online
DOI: 10.1039/C6RA09033H

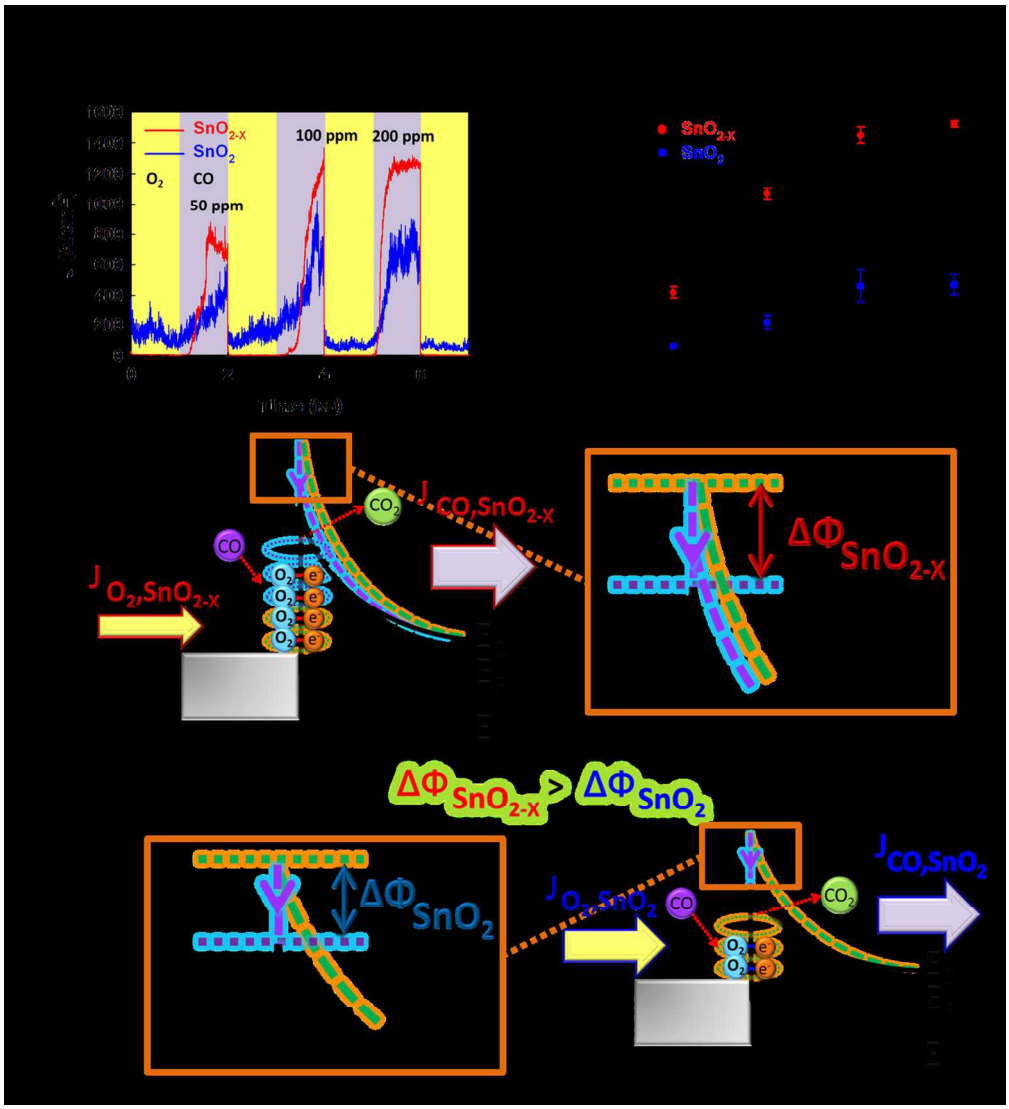

Figure.3 (a) represents detection performance of O2 with different CO concentration sensing at 200 oC operation temperature. (b) The sensitivities of SnO2-X NW device are higher than SnO2 NW device for different CO concentrations detection. (c) shows the detection mechanism of SnO2-X and SnO2 NW devices. Considering CO/O2 alternate-detection, the SBH variation of SnO2-X NW device is larger than SnO2 NW device (ΔΦ SnO2-X > ΔΦ SnO2), that is due to the high surface VO density of SnO2-X NW device.
255x280mm (150 x 150 DPI)